Received 11 May 2022; revised 14 June 2022; accepted 20 June 2022. Date of publication 28 June 2022; date of current version 8 July 2022.

Digital Object Identifier 10.1109/OJAP.2022.3186643

A Review of Magnetic Field Emissions From the Human Body: Sources, Sensors, and Uses

KEREN ZHU (Student Member, IEEE), AND ASIMINA KIOURTI (Senior Member, IEEE)

ElectroScience Laboratory, Department of Electrical and Computer Engineering, The Ohio State University, Columbus, OH 43221, USA

CORRESPONDING AUTHOR: K. ZHU (e-mail: zhu.1266@osu.edu)

ABSTRACT It has long been common practice to capture the electric fields emanated by the human body as a means of detecting and/or monitoring diverse health conditions. However, these electric fields are strongly impacted by the complex permittivity of biological tissues which deteriorates their waveforms and limits their diagnostic capabilities. As an alternative, recent progress has been made in the measurement of bio-magnetic fields occur from the natural currents flowing through the body. The advantage in this case is, since tissues are non-magnetic, magnetic fields propagate in an uninterrupted manner towards the skin surface where they are eventually collected. This unveils game-changing opportunities for future medical diagnostics. Nevertheless, a major challenge associated with sensing these naturally emanated magnetic fields is that they are extremely weak, and in fact orders of magnitude smaller than those generated by the Earth. To this end, extensive efforts have been pursued to realize sensing technology that is sensitive enough to collect bio-magnetic fields. Example fields of use include magnetomyography (MMG), magnetocardiography (MCG), magnetoencephalography (MEG), and Magnetoneurography (MNG) (including magnetospinography (MSG)). This review will provide an overview of technologies used to sense bio-magnetic fields, list their merits and limits in a critical manner, and discuss clinical applications.

INDEX TERMS Bioelectromagnetics, magnetocardiography (MCG), magnetoencephalography (MEG), magnetomyography (MMG), magnetoneurography (MNG), magnetospinography (MSG).

I. INTRODUCTION

THE HUMAN body consists of more than 200 types of cells and four different types of tissues where the action potential impulses propagate through. These electrically mediated signals travel along the axon as the ions flux in and out of the membrane forming various electrophysiological activities in the human body that gives rise to electric and magnetic fields [1]. These currents are responsible for the electrophysiological activity in the human body that gives rise to electric fields. Examples of sensing these electric fields include electrocardiography (ECG) for the heart and electroencephalography (EEG) for the brain [2]. However, However, electric signals can be greatly impacted by the complex permittivity and conductivity of biological tissues, leading to inaccurate diagnostic results [3]. In addition, devices that capture bio-electric fields rely on electrodes that are in direct contact with the skin or scalp, making the procedure intrusive [4]. Most importantly, the electric signal can only provide limited information. Complimentary features of the magnetic signals, such as field localization and vortex current identification, can help accelerate diagnostic procedures and provide more accurate diagnosis.

An alternative way is to measure the magnetic fields produced by the aforementioned ionic currents. Examples include magnetic fields radiated by the muscles (magnetomyography, MMG), heart (magnetocardiography, MCG), brain (magnetoencephalography, MEG), and nerves (magnetoneurography, MNG, such as from the spine, magnetospinography, MSG). Since biological tissues have magnetic permeability similar to vacuum, bio-magnetic fields can propagate to the surface of the skin without any distortion [5]. In addition, bio-magnetic fields can be captured in a non-contact manner, in turn eliminating obtrusiveness, skin irritation and possible allergic reactions [6]. However, the main challenge associated with capturing these magnetic waves is their extremely weak field strength and wide bandwidth. Referring to Table 1 and the example waveforms in Fig. 1 (original figures available in [7]–[11]),

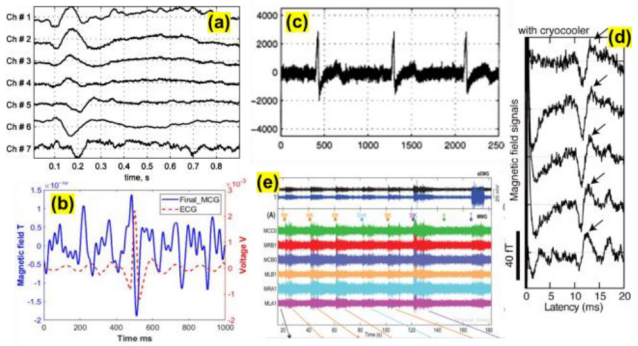

FIGURE 1. Example bio-magnetic signal waveforms for different source: (a) Brain (MEG): 7 channel auditory MEG [7]; (b) Heart (MCG): MCG vs. ECG signal measured without shielding [8]; (c) Nerve (MNG): raw measurement of evoked MNG in the peripheral nervous system [9]; (d) Spine (MSG): evoked MSG waveforms with cryocooler applied to SQUID sensor [10]; and (e) Muscle (MMG): MMG of the levator ani muscles during pregnancy [11].

TABLE 1. Bio-magnetic signal features for different sources.

Source	Range	Frequency	Bandwidth
Brain (MEG)	100 fT – 1 pT	0.5 - 500 Hz (clinically relevant <70Hz)	~500 Hz / 70 Hz
Heart (MCG)	50 -100 pT	<75 Hz	75 Hz
Nerve (MNG)	5 fT – 8 pT	6-500 Hz	494 Hz
Spine (MSG)	1 – 100 fT	100-5000 Hz	4900 Hz
Hand/Leg/ Head Muscle (MMG)	1 fT – 1 pT	1-300 Hz	300 Hz

their frequency ranges from couple Hz to thousands of Hz and their magnitude is in the range of 10^{-10} T to $\sim 10^{-15}$T at the recording site [9], [10], [12]–[20]. That is orders of magnitude lower than the earth's magnetic field (10^{-4} T) [21], [22].

Given the difficulty in capturing such weak signals, original focus had been on solely capturing bio-electric fields [23]. However, this changed when extremely high sensitivity magnetometers were introduced, namely superconducting quantum interference devices (SQUIDs) [24], alongside magnetic shielding techniques (e.g., high permeability materials, such as Mu metal and Metglas) [25]. However, SQUIDs operated in shielded rooms are bulky and extremely expensive [26]–[28]. They also require cooling structures or liquid helium to maintain subzero temperatures (i.e., below 80K [29]), which further increases complexity and cost [26]. These can only be partially mitigated via novel approaches that employ different cryogen (such as nitrogen) and cryocoolers [26], [30]. More recently, other types of magnetometers or gradiometers have been developed for bio-magnetic field sensing, aiming to overcome limitations of SQUIDs [8], [31]–[33]. These sensors can be mainly categorized as: Atomic Magnetometers (AM), including Optically Pumped Magnetometers (OPM) and Spin Exchange Relaxation Free Atomic Magnetometers (SERF AM), and induction coil gradiometers. Here, to achieve the desired sensitivity, most of the sensors require some

FIGURE 2. (a) Operation principle of a typical SQUID. (b) A SQUID system in superconducting magnetic shield [58].

sort of shielding. This can be either partial shielding upon a targeted region [34] or complete shielding in the form of a shielded room where measurements are taken in [35]–[37]. Even more recently, promising results have been reported for recording bio-magnetic fields in non-shielded environments [8], [38]–[40]. These approaches take advantage of advanced Digital Signal Processing (DSP), including, but not limited to: bandpass filtering, window averaging, moving averaging filtering [8], [40], and integration of a feedback mechanism to lower magnetic noise in the final processed data [41]–[43].

In this paper, we review the state-of-the-art technology in bio-magnetic field sensing, including both sensors and shielding techniques. Merits and limits of these approaches are presented in a critical manner. We also discuss the sources and clinical value of MMG, MCG, MEG and MNG (MSG), as well as provide example technologies used to capture these signals. To our knowledge, this is the first paper that reviews bio-magnetic field sensing and related technologies. Our ultimate goal is to familiarize readers with the state-of-the-art and inspire new technology development and clinical uses in this area.

II. STATE-OF-THE-ART-TECHNOLOGY

A. SUPERCONDUCTING QUANTUM INTERFERENCE DEVICES (SQUIDS)

SQUIDs are the most commonly used devices for sensing bio-magnetic fields [44]. They operate based on the principles of Josephson Junctions, electron quantum tunneling, and the idea that magnetic flux through a superconducting loop is quantized [45]. A typical SQUID consists of two parallel Josephson junctions forming a circular loop from two superconductors separated by two thin insulating layers, per Fig. 2 (a). A constant biasing current is applied and maintained in the circular loop making each side of the loop having half of the total current. As the bio-magnetic flux goes through the loop, the current caused by the magnetic flux is added on the original half of current on one side of the loop, whereas on the other side, the flux current is removed from the original half. This leads to phase difference between the junctions, making one side of the junction reach the critical current (i.e., maximum current that can pass through the junction) before the other one. Based on the quantization of magnetic flux, the voltage is oscillating

TABLE 2. Relevant parameters for SQUIDs.

Ref	Detection level	Signal	Sensor	Shield	Frequency [Hz]	Noise [fT/√Hz]
[50]	~10 pT	MCG	Low-Tc SQUID (research)	No	1 100	20 8
[51]	~10 pT	MCG	High-Tc SQUID (research)	No	1 10	100 40
[38] [39]	~10 pT	MCG	Low-Tc SQUID MAG-SKAN SQUID (Commercialized)	No	10 100 354	~6 ~1 0.5
[35] [36]	~100 fT	MEG	High-Tc SQUID (research)	Yes	10 100	50-130 ~100
[52] [53]	~800 fT	Evoke MEG	High-Tc SQUID (research)	Yes	White noise	~ 7
[52] [53]	~800 fT	Evoke MEG	Low-Tc SQUID Magnes 3600WH (Commercialized)	Yes	White noise	~ 5
[54] [19]	~800 fT	MMG	SQUID for reproductive assessment i.e. SARA (Commercialized)	Yes	10 100	~ 10 ~ 4.4
[20]	~8 pT	MMG	SQUID for reproductive assessment i.e. SARA (Commercialized)	-	-	-
[55]	~3.5 fT	Evoke MSG	SQUID Magnes 1300C (Commercialized)	Yes	>5	<10
[56] [57]	<10 fT	Evoke MSG	Low-Tc SQUID (Research)	Yes	White noise	<3

between the maximum and minimal value of the quantum where the maximum values are happening at integer values of the flux quantum and the minimal values are happening at half integer values of the flux quantum. Counting the oscillations/changes in voltage, magnetic flux changes can be evaluated.

For biomagnetism, two different types of SQUID sensors have been typically used, viz. High-Tc and Low-Tc, as based upon their operating temperature. Earlier studies and commercially available devices use low-Tc SQUIDs that operate on high-cost liquid helium cooling systems at ~4K [46]. More recent works introduced high-Tc SQUIDs [26], [29] that operate at ~77K [26] using a liquid nitrogen cooling system to reduce operational cost. A trade-off here is that high-Tc SQUIDs tend to have worse noise performance than the low-Tc SQUID counterparts, roughly a noise figure of one order of magnitude lower [47]. Nevertheless, noise performance may ultimately not impact the lowest biomagnetic signal that can be captured [47]: because of their higher operation temperature, high-Tc SQUIDs have less thermal insulation, leading to smaller distance between the signal source/subject and the cooled sensor, thus enhancing the signal strength that is fed into the SQUID. As a result, the final signal to noise ratio (SNR) can be comparable between high-Tc and low-Tc SQUIDs [48]. Table 2 summarizes SQUID designs and their performance, noting that extensive work has been pursued towards improving upon the original concept and enabling higher sensitivity, lower cost, more compact design, and larger bandwidth [19], [35], [36], [38], [39], [44], [49]–[57]. As seen, SQUIDs are extremely sensitive and able to detect magnetic fields as low as pT to fT. As expected, low-Tc tend to have lower noise floor: their noise performance typically lies in the range of 1-10 fT/$\sqrt{}$Hz at ~10 Hz. For some low-noise low-Tc SQUIDs, noise can go down to <1 fT/$\sqrt{}$Hz at ~100 Hz. On the other hand, for high-Tc SQUIDs, noise lies in the range of 10-100 fT/$\sqrt{}$Hz at ~10 Hz.

Key limitations associated with SQUID sensors entail:

a) High cost and bulkiness. Besides the cost of the device itself, operation becomes further expensive due to the use of cryogenic cooling [30]. Cost is also exacerbated by the 20-ton shielding room needed to accompany the device, made of multiple layers of expensive high-permeability alloys [44], [56]. A detailed description of shielding technologies is provided in Section II-D. Fig. 2(b) shows a typical SQUID system in a superconducting magnetic shield (original figure available in [58]). As seen, the size of the sensor itself is already very bulky. On top, the shielding room introduces substantial additional volume.

b) Sophisticated fabrication, especially for high-Tc SQUIDs. Per Table 2, commercially available SQUIDs all rely on the principle of low-Tc. One important factor that limits the commercialization of high-Tc SQUIDs is the poor fabrication yield and low reliability [48], [59]. Typical low-Tc SQUIDs use Nb-based nano-SQUID technology, where the fabrication process is already mature for large scale manufacturing [60]. For high-Tc SQUIDs, the most promising fabrication method utilizes grain boundary junctions based on $YBa_2Cu_3O_{7-x}$ (YBCO) thin films [61] deposited on $SrTiO_3$ (STO) or $LaAlO_3$ (LAO) [62], [63]. More recent works report the use of ion beam milling to fabricate these nanojunctions [61], [64]. Both fabrication processes are very challenging and only a small number of labs have the ability to produce them with high enough quality [26], [65]. As a result, though high-Tc SQUID sensors seem to be a better alternative to low-Tc in terms of cost, progress needs to be made to empower their wide adoption.

B. ATOMIC MAGNETOMETERS (AM)

Two types of AMs, specifically Optically Pumped Magnetometer (OPM) and Spin Exchange Relaxation-Free (SERF), rival the SQUID sensors in terms of performance under certain conditions. Both AMs operate

TABLE 3. Relevant parameters for AMs.

Ref	Atom	Signal	Sensor	Temp. ºC	Frequency [Hz]	Noise [fT/√Hz]
[37]	^{4}He	MCG	OPM	Room temp.	2-300	Average: 210
[69]	Rb	MCG	OPM	150	10 1	~30 ~100
[70]	K	MCG	SERF	180	10	38
[71]	Rb	MEG	SERF	150	60-80 10	Ave: 15.6 ~100
[72]	K-Rb	MEG	OPM	180	10	18.4
[73]	K	MEG	SERF	-	10	3.5
[74]	K	MEG	SERF	160	10 25-100	10 6
[75]	Rb	Evoke MEG	SERF	150	2-40 10-100	14.46 5
[76]	K	MEG (alpha band eye open)	SERF	180	10 100	21 ~50
[77] [78]	^{87}Rb	Auditory evoke MEG	OPM (Commercialized QZFM QuSpin)	150	>1	10
[79]	Rb	MMG	OPM (Commercialized QuSpin)	-	1-100	15
[80]	Rb	Muscle Action Potential (MAP)	OPM (Commercialized QZFM QuSpin)	-	3-135	15
[81]	Rb	MMG	OPM (Commercialized QZFM QuSpin)	150	10-150	≤25

on a similar principle, i.e., heating atoms to a high temperature and detecting the magnetic attenuated atomic spins via pumping and probing of the optical system. Most AMs require alkali atoms such as K, Rb, and Cs to be vaporized by heating them up to a certain temperature, typically 100-190 °C [66]. These vaporized alkali atoms interact with the magnetic field such that, by detecting the atomic spins, the corresponding magnetic field can be identified [67], [68]. More specifically, vaporized alkali atoms are first circularly polarized so that they spin alone in the same direction. The target magnetic fields interact with the polarized atoms, causing precession of their magnetic moment, which can be used to infer the magnetic field [67]. SERFs, as the name suggests, differ from OPMs as they are free from decoherence due to spin exchange collision. This is typically achieved by elevating the temperature of the cell to increase the density of alkali metal atoms and eventually the rate of spin exchange collision so that it exceeds the Larmor Precession Frequency [68]. We remark here that, though this principle describes traditional AMs, recent works have improved upon this technology in many ways (i.e., in terms of the atoms used) [37]. Comparing the two, SERF AMs surpass OPM by exhibiting much higher sensitivity.

Table 3 summarizes AMs that have shown to successfully capture human bio-magnetic signals [37], [69]–[81]. As expected, SERF AMs have better sensitivity when compared to OPMs. Notably, some of the most recent SERFs can achieve noise performance of around 10 fT/$\sqrt{}$Hz at ∼10 Hz which is comparable to most of the high-Tc SQUID sensors. In fact, theoretical studies have shown that SERF AMs could replace SQUIDs in the future [67], [82], [83], with some even claiming that SQUIDs have already been surpassed [67]. Comparing AMs to SQUIDs, we note that: (1) AMs do not require any type of cooling structure; (2) AMs significantly reduce the operational cost as the device itself is less expensive, shielding is less complex, and no coolant is required [44], [84]; (3) AMs are very small in size. For example, Fig. 3 (original figures available in [85], [86]) shows the typical size of an OPM and SURF. Most of AMs are just couple centimeters in their largest dimension [34], [37], [66], [74].

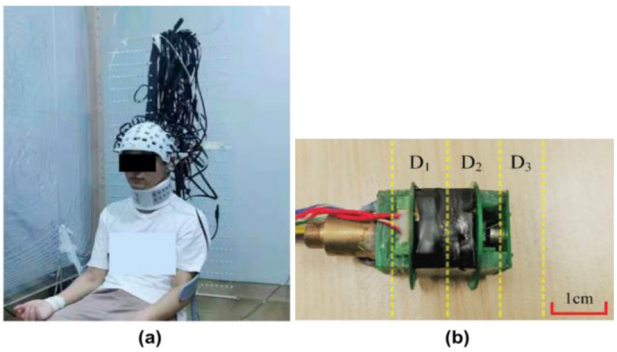

FIGURE 3. (a) 31 channel OPM sensor placed on a helmet [85]. (b) SERF magnetometer probe [86].

Nevertheless, AMs still suffer from a number of limitations. One of the fundamental drawbacks is that they can only operate near zero ambient magnetic field [68]. For example, to implement the SERF state, the external stray magnetic field needs to be <10 nT or ideally zero [68]. To date, all types of AMs require magnetic shielding to maintain near zero ambient noise for ultra-high sensitivity [67], [77], with some options being more affordable than others [34], [77]. As another drawback and due to theoretical limitations, AMs have extremely small bandwidth [83], restricting the biomagnetic signals that can be captured. Another concern is related to safety as AMs are placed on top of/near the skin, where the sensor temperature can reach up to 65 °C [81]. Finally, the pump and probe laser that are used to polarize

TABLE 4. Relevant parameters for induction coil gradiometers.

Reference	[40]	[87] [88]	[8]
Noise measured	104 fT/√Hz	3.4 pT	70 pT/√Hz
Frequency	10 Hz	18 Hz	10 Hz
Coil outer diameter D	70 mm	120mm	15 mm
Coil inner diameter Di	20 mm	60 mm	9.3 mm
Coil length H	60 mm	30 mm	11 mm
Core material	Ferromagnetic	Air	Air
Shielding	Y/N	Y	N
Signal captured	MCG	MCG	MCG
Signal visibility	Clear	Not clear	Clear

and detect the atomic spin make the procedure non-passive and may lead to safety concerns as well.

C. INDUCTION COIL GARDIOMETERS

Induction coil-based gradiometers rely on the simple principle of Faraday's law that changing magnetic field can induce voltage upon a coil's ends. This voltage can then be translated back to the magnetic flux being induced. Work reported in this area is very limited mainly due to high intrinsic noise. Nevertheless, recent works have shown the potential of capturing MCG activity (the strongest bio-magnetic field generated by the human body) using relatively lightweight and small coil sensors [8], [40], [87]. Table 4 compares the relevant parameters reported in [8], [40], [87], [88]. In terms of the sensor's physical design, ferromagnetic cores [40] and optimal coil size/ratios [8], [40], [87] are used to boost sensitivity. For example, in [87], [88], the optimal coil size was chosen such that inductance (L) is maximum at a fixed winding length (similar to designing Brooks-Coils). However, this approach is not as effective when designing for a low noise bio-magnetic gradiometer. Based on the model developed in [87], [88], sensitivity (S) is defined as the induced voltage (V_{out}) vs. magnetic field strength (H). Note that S is always proportional to the coil winding (n) and coil mean radius (Ra), regardless of the operation frequency. However, fixed winding length doesn't mean fixed Ra and n. Also, L depends on the coil geometry, meaning that different Ra and n values lead to different L. In turn, different L also leads to different Ra and n values. Therefore, all variables are not independent of each other and the exact relationship between L and S is not clear without considering other parts of the coil parameters. The work in [8] and [40] uses a similar approach to determine the optimal coil geometry ratios. Ferromagnetic core is used in [40] to boost the coil sensitivity at the expense of increasing the sensor's weight. Comparing the two, (1) [40] is estimated to be at least 216 times heavier than [8], (2) [40] is significantly larger in size; but (3) [40] has better noise performance.

Table 5 compares the output voltages (Vout) and thermal noise (Vt) from coils with same outer diameters using the aforementioned three designs. Ideally, we want the gradiometer to be as small as possible with high output voltage and low thermal noise. Here, optimal coil geometry ratios from [8], [40], [87] are used to calculate the exact coil size. Vout and Vt are calculated using a tightly winded air-core coil model. Indeed, for a given 1 pT 40 Hz magnetic field, Brooks coil designs (i.e., [87], [88]) have shown to have the smallest output voltage and smallest Vout:Vt ratio. Further, [8] and [40] have very similar performance with [8] while also exhibiting a better Vout: Vt ratio.

TABLE 5. Induction coil gradiometer performance comparison.

Reference	[40]	[87] [88]	[8]
Coil outer diameter D	12 cm	12 cm	12 cm
Coil inner diameter Di	5.1 cm	6 cm	6.7 cm
Coil length H	8.28 cm	3 cm	8.6 cm
Wire diameter a	0.23 mm	0.23 mm	0.23 mm
Wire material	Cu	Cu	Cu
Vout at 1pT 40 Hz	77.9 nV	27.2 nV	74.3 nV
Thermal noise Vt at Δf=1	9.83 nV	5.66 nV	9.18 nV
Ratio Vout:Vt	7.93	4.81	8.10

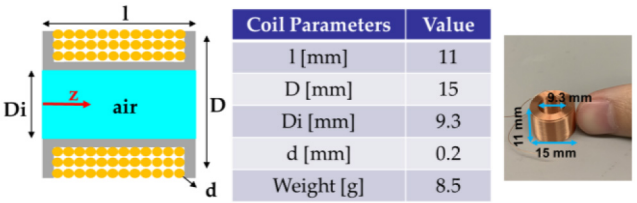

FIGURE 4. Induction coil gradiometer proposed in [8].

Compared to SQUIDs and AMs, induction coil gradiometers have the following advantages. (1) Operation cost is significantly reduced as no shielding or coolant are needed and the sensor itself is very inexpensive. (2) Size is comparable or smaller to that of a typical compact AM sensor. As an example, Fig. 4 shows one of the developed induction coil sensors (original figure available in [8]). (3) Portability is enhanced as there are no shielding requirements. (4) There is no theoretical constraint in terms of bandwidth. (5) Operation is fully passive. (6) There is no requirement for cooling or heating structures.

The only limitation of induction coil gradiometers relates to their noise performance. In unshielded environments, noise performance of an induction coil gradiometer is about 10 times worse than that of a typical OPM or high-Tc SQUID in a shielded environment. As a result, to date, even with adequate filtering and signal processing, induction coil gradiometers are only capable of capturing MCG signals when averaging the data for couple of minutes. However, not much work has been done using this technology yet, and the area is still developing and expanding. Future directions in this area may involve integrating machine learning, advanced signal processing, and partial shielding to optimize the system.

D. SHIELDING TECHNOLOGY

Magnetic shielding rooms (MSRs) are often used in addition to sensing systems to reduce the background noise that is present when recording bio-magnetic fields. Two types of MSRs are commonly used that rely on active and passive shielding, respectively. As the name suggests, passive shielding utilizes only passive components, typically multiple

layers of high permeability materials. Active shielding adds components, such as multiple demagnetization coils, to the traditional passive shielding to further calibrate the remaining noise [33], [44], [73].

For direct-current (DC), MSRs rely on ferromagnetic materials with high permeability to create a preferential path for the magnetic field lines, shunting the magnetic flux and drawing the field into themselves. For alternating current (AC), MSRs utilize eddy currents induced on a conductive plate to cancel out the external magnetic noise [89]. For most bio-magnetic applications, MSRs that utilize ferromagnetic shunt (i.e., DC operation principle) alone, can provide sufficient shielding [90]. This is because, though the environmental noise contains both DC and AC components, the AC noise of interest (overlapping with the bio-magnetic signal) is slowly varying. With frequencies lower than a few hundred kHz, the eddy current induced on the conductive plate cannot effectively cancel out the external noise due to loss. Therefore, for human emitted bio-magnetic fields that focus on low-frequency noise, ferromagnetic material MSRs are typically used.

Nevertheless, active shielding can be used in conjunction with passive MSRs. In this case, coils are typically added to the outside of the passive MSRs to compensate the noise [91], [92]. Active shielding systems work by sensing the noise using multiple gradiometers on the outer layer of the passive MSR. The recorded noise is then compensated by multiple coils within the compensation system. Currently, traditional MSR together with active shielding is the primary configuration used in the field of bio-magnetism.

To numerically measure shielding ability, the concept of shielding factor (SF) is introduced. This is calculated as the ratio of the magnetic field induced when no shielding is present (B_0) over the magnetic field induced at the same location when shielding is present (B) [93]. Higher SF indicates higher level of shielding. To design rooms with high SF for bio-magnetic applications, two factors are critical: shape/dimensions and material. For a typical cylindrical or spherical shaped shield, several studies have discussed the theoretical optimal design, and for each case, SF has been calculated [94], [95]. For materials, a general rule is to use materials with high permeability [90]. One of the materials that is widely known for good shielding performance is called "Mu" material and is an alloy of nickel and iron. Different compositions can produce variations of Mu materials, all of which have high permeability and can be used for bio-magnetic shielding. Example compositions include: 80% nickel, 4.2% molybdenum, 0.5% manganese, 0.35% silicon, 0.02% carbon and 15.03% iron (i.e., HyMu 80) [90], 80% nickel, 4.6% molybdenum and 15% iron [96], 80.5% nickel, 4.9% molybdenum and 13.7% iron [96], 77.9% nickel, 4.5% molybdenum, 3.5% copper and 13.2% iron [96], and 79.7% nickel, 15% iron, and 4.6% molybdenum [97]. Nevertheless, more recent studies show that several layers of high magnetic permeability metals can attenuate the external fields, limiting the shielding ability [98]. New materials such as MnZn ferrites are studied as a promising alternative [98].

III. APPLICATIONS

In this Section, we report clinical applications that rely on bio-magnetic field sensing, and specifically MCG, MEG, MNG/MSG, and MMG. These applications are, of course, not limiting and the field is ever expanding.

A. MAGNETOCARDIOGRAPY (MCG)

Fig. 1(b) (original figures available in [8]) shows the MCG signal superimposed with an ECG signal. Key features of the wave consist of the P, Q, R, S, T, U spikes, where the QRS complex is the most prominent feature (main spike) lead by the P spikes and followed by the T and U spikes. MCG empowers advanced diagnostics of various cardiac-related health conditions in clinical settings (e.g., arrhythmia [99], [100], cardiac ischemia [99], [101], right atrial hypertrophy [102], coronary artery disease (CAD) [103]–[105], and Brugada syndrome [102]). Referring to CAD, one of the most common heart conditions, limitations of traditional ECG that can be overcome by MCG entail:

(a) Difficulties in diagnosing symptomatic patients without persistent ECG features (i.e., ST-segment elevation) [105]. By contrast, MCG is highly sensitive towards tangential and vortex currents that cannot be detected in ECG [103], enabling better detection of CAD with the DC injury current (note that injury current is slowly decaying (near-DC) current) [106].

(b) Low sensitivity/accuracy in detecting ECG property changes, particularly for rest-ECG, implying that several patients need to undergo expensive and invasive diagnostic procedures [100]. By contrast, MCG provides a well-defined change, especially on the ST segment and T wave. Given these well-recognizable markers on MCG, research shows that MCG can achieve twice as high success rate for Sensitivity (Sens) and Negative Predictive Value (NPV) (i.e., 95.1% vs. 33.9% and 84.8% vs. 27.4%) while having slightly higher Specificity (Spec) and Positive Predictive Value (PPV) as compared to its ECG counterpart (i.e., 92.8% vs. 91.1% and 97.8% vs. 93.3%) [107].

(c) Lack of field localization which, in turn, may prohibit localization of coronary stenosis. By contrast, MCG provides much more localized fields and detailed 3D imaging over the heart so that the exact location of coronary stenosis can be detected. Research also shows that other MCG features, such as magnetic pole characteristics, are also associated with location identification [108].

In other cases, MCG has been explored for prognostic and monitoring tests [100], [109]–[114]:

(a) *Arrhythmogenic risk assessment:* Arrhythmia is the leading cause of sudden cardiac death (SCD); therefore, prevention is of crucial importance [115]. MCG features that can be extracted for arrhythmogenic risk evaluation include

the late field, intra-QRS fragmentation, and QT dispersion (QTd) [111], [116]–[118]. The late field refers to small abnormal deflections at the end of the QRS wave. Studies have found late field parameters extracted from MCG to discriminate post-myocardial infarction (MI) patients who had arrhythmia (ventricular tachycardia (VT)) from those who hadn't [111] and to distinguish patients with early repolarization patterns (ERP, known as a risk factor for ventricular fibrillation (VF)) [119]. Compared to late fields extracted from signal averaged ECG (SAECG), MCG late fields provide more accurate prognosis of VT in post-MI patients [111]. Intra-QRS fragmentation refers to the high frequency components in the QRS region [120]. It can be quantified through the number of peaks (M) within the QRS and the intro-QRS fragmentation score (FRA) which is calculated as the product of peaks and the sum of the peak amplitudes [121]. Studies have found both M and FRA extracted from MCG to predict arrhythmic events, VT, and even all-cause mortality in post-MI patients [116], [121], [122]. Compared to SAECG intra-QRS parameters, MCG intra-QRS has higher specificity rate (100% vs. 91%) while having the same sensitivity (95%) [121]. Finally, QTd measures the difference between the maximum and minimum QT duration [117]. Studies have shown evidence that increased QTd can identify post-MI patients at risk for malignant arrhythmia, predict long-term prognosis in acute myocardial infarction (AMI) and even serve as a predictor of SCD [117], [118], [123].

(b) *Rejection monitor:* MCG shows promising results in monitoring post heart transplantation patients for rejection reaction. Traditionally, transplant rejection is monitored via serial cardiac endomyocardial biopsy (EMB) where a small myocardial tissue is obtained with an invasive procedure [124]. Studies have shown MCG mapping to non-invasively test/monitor for rejection reaction using the intensity of the equivalent current dipole (ECD) [124], [125]. In fact, it can detect acute graft rejection reaction as early as EMB with possibly higher detection rate. However, up to now, studies have very limited sample size (i.e., up to 15 patients) and further explorations are needed [126].

(c) *Fetal MCG (fMCG):* fMCG monitors the fetus's cardiac activities outside the maternal abdomen, which can serve as a diagnostic and prognostic tool for the baby. It can be used for several applications, such as: detection and classification of fetal arrhythmia, detection of congenital heart diseases, first-degree atrioventricular block, fetal long QT syndrome, fetal Wolff-Parkinson-White syndrome, and more [30], [127], [128]. This is made possible by the fMCG's ability to clearly show all parts of the P, QRS, and T waves. As biological tissues have magnetic permeability similar to that of free space, fMCG can propagate relatively undisturbed through the body. By contrast, other commonly used fetal surveillance tests only provide mechanical assessment of heart rhythm which is not sufficient for diagnosis (i.e., echocardiography), are non-passive and may cause safety concerns (i.e., fetal MRI), and are unreliable (i.e., fetal ECG which, due to tissue attenuation, can only record cardiac signals with adequate information in about 50% of the cases). fMCG surpasses these approaches with the ability to provide good quality P, QRS and T waves information in normal pregnancies from the 20^{th} week onward with a success rate close to 100% [129]. In some studies, it is shown that fMCG can be recorded as early as the 13^{th} week of gestation [130].

B. MAGNETOENCEPHALOGRAPHY (MEG)

MEG has shown to achieve similar accuracy in localizing epilepsy as compared EEG [131]–[133]. Fig. 1(a) (original figures available in [7]) shows an example auditory MEG where the spikes indicate activation of the brain. Notably, for patients with temporal lobe epilepsy, MCG offers higher sensitivity as much smaller brain activation areas are required for epileptic spikes detection as compared to scalp EEG (6-8cm^2 vs. 20-30cm^2) [134], [135]. In addition, MEG is particularly useful for patients with frontal lobe epilepsy and neocortical epilepsy, as studies show that MEG offers higher spatial resolution and better signal-to-noise ratio, as well as yields significantly higher spike rate than EEG, hence facilitating advanced source localization [133], [136].

In other cases, fetal MEG (fMEG) has been reported as a non-invasive means of monitoring brain electrophysiology. It can assess the maturation of different parts of the fetal brain (i.e., auditory evoked field, visual evoked field) which can serve as prenatal assessment, including diagnosis of developmental delays [137]–[139]. This information can't otherwise be extracted with fetal EEG (fEEG) and invasive procedures are needed instead that place electrodes close to the head of the fetus [139]. In turn, fEEG studies are primarily focused on primates (sheep) and postnatal newborns [140], [141].

MEG is also known for presurgical and preoperative evaluation, especially for epilepsy, focal cortical dysplasia (FCD), and brain tumor surgery [142]–[144]. Studies show that MEG can provide more localized epileptogenic zoom and can detect locations that might otherwise be missed if only evaluated through EEG or MRI [145]. Information provided with MEG, though not required for presurgical evaluation, has been demonstrated in several studies to provide favorable outcomes (i.e., seizure free, localized resection volumes) [146]–[148]. For space occupying lesions, such as tumors, pre-operative functional mapping using MEG can help reduce intraoperative time, positively impact the extent of resection, and improve patient outcomes [149]–[151].

In other cases, studies show the potential of using different activation patterns within MEG to serve as biomarkers of differentiating between different emotions/feelings [152], [153] (e.g., neural activity from the primary somatosensory cortex in MEG at $\sim$10 Hz is shown to link to pain stimuli [154], MEG theta band (4-8 Hz) signal patterns in the amygdala are shown to vary when exposed to angry, fearful and neutral faces [155]). Additionally, MEG-based technologies have been reported that quantify cognitive workload with the auditory steady-state response (ASSR) [156]; control brain computer interfaces (BCIs) with higher accuracy than EEG

TABLE 6. MNG and MSG excitation and recording sites.

Ref	Excitation	Recording	Max field	Peak latency
[159]	Nerve at the knee	L5/S1 foramen	60 fT	8.25-8.95 ms
[160]	Rabbits sciatic nerve	Lumbar spinal cord	240.24 fT	110.7±16.5 ms
[161]	Median/ulnar nerve	Dorsal neck	-	-
[162]	Wrist median nerve	Neck	-	-
[163]	Lower thoracic cord	Cervical spine	~25 fT	Speed: 64.3 m/s
[163]	Elbow median nerve	Cervical spine	~50 fT	Speed:53.3-120 ms
[164]	Wrist ulnar nerve	C6/7 - T1/2 intervertebral foramina	30±7.8 fT	11.5±0.8 ms
[164]	Elbow ulnar nerve	C6/7 - T1/2 intervertebral foramina	64±12 fT	7.5±0.4 ms
[165]	Wrist median nerve	Neck	-	-

when it comes to multiple tasks with activities corresponding to distinct brain area [157]; and move a tetraplegic patient's index finger [158].

C. MAGNETONEUROGRAPHY (MNG) AND MAGNETOSPINOGRAPHY (MSG)

MNG and MSG are both developing technologies. Though not approved for clinical use yet, several studies have shown their potential for peripheral nerve and spinal cord applications in the future. Specifically, one potential application for MSG/MNG relates to visualizing spinal cord injury. Studies have found that evoked electrophysiological activities can be detected though MSG and MNG in various locations along the spinal cord. This indicates the potential of using MSG and MNG as a noninvasive tool for visualizing neural activity in the cauda equina [159], examining lumbar diseases [159], localizing lesion site in the lumbar canal [160], diagnosing conduction block even at the site of spinal stenosis in cervical myelopathy patients [161]–[163], detecting spinal root and dorsal horn dysfunction [163], visualizing ulnar nerve stimulation at spinal tracts at C5/6/7 [164], and measuring neural activity in the dorsal column and dorsal horn in the cervical cord [165]. Since nerves serve as a pathway for transmitting signals, MSG and MNG are essentially recording the evoked potential traveling through the nerve. The stimulation typically involves external electrical stimuli applied to one end of the nerve and recording on the other end. Example stimulation and recording sites that have proven to be able to record evoked MSG/MNG together with their corresponding signal strength and peak latency are summarized in Table 6. Fig. 1(c) and Fig. 1(d) (original figures available in [9], [10]) are examples of evoked MNG and MSG where each spike in the waveform is followed by the applied stimuli. The time difference between the applied stimuli and the appearance of the spike is called the peak latency. Here, the peak latency characterizes how fast the signal travels along each specific nerve. It can be used to check if there is any damage to that nerve pathway. Though only a very limited spinal nerve paths have been studied to date, MNG/MSG still show huge potential for numerous spinal related clinical applications.

Applications of MSG/MNG beyond the spinal cord have also been demonstrated. Specifically, the technology has been used to diagnose and localize conduction block in brachial plexus neuropathy [166], detect lesions proximal to Erb's point in peripheral nerves [167], visualize neural activity in the brachial plexus [168], diagnose and localize focal neuropathies of cervical nerve roots [169], and diagnose functional electrophysiological somatosensory pathways [170].

Comparing MSG/MNG to traditional clinical practices, one key advantage is that MSG/MNG can detect electrophysical activities in the nerve non-invasively. By contrast, to detect electrical potential in the nerve, conventional approaches need to surgically identify the nerve and place the recording electrode which introduces numerous complications.

D. MAGNETOMYOGRAPHY (MMG)

MMG can be used to detect magnetic fields from muscles and has been demonstrated to achieve superior performance than gold-standard electromyography (EMG) on several occasions. Example applications include remote detection of mechanical/metabolic injury-related slowly decaying leakage/injury currents [171]; detection of female pelvic floor function associated with the contraction of levator ani muscle [19]; prediction of labor with uterine activity [20], [172], [173]; analysis of the muscular activity of the arm and study of the innervation of the hand [34], [174]. Fig. 1(e) (original figures available in [11]) is an example of recorded levator ani muscles MMG side by side with the EMG during pregnancy. Each spike in the EMG has a corresponding spike in the MMG indicating the muscle contraction.

Among the above, one of the most studied applications of MMG is the detection/prediction of labor using uterine activity. MMG can measure the electrophysical activities of the uterine, extract information from action potentials in groups (bursts) related to the characteristic of uterine muscle contraction (i.e., frequency, duration, and number of simultaneously active cells), and, hence, a predict labor [20]. Analyzing uterine contractions and predicting labor could be useful clinically, especially for early identification and prevention of patients for premature delivery [20], [173].

Currently, the most common approaches for labor prediction are intrauterine pressure catheter (IUPC), tocography (TOCO), and EMG. Comparing those approaches to MMG, IUPC and EMG are invasive. IUPC requires a catheter inserted into the uterus and rapturing of the amniotic membranes to measure the pressure changes [175], while EMG uses both internal electrodes and abdominal surface electrodes in direct contact with the patient [175], [176]. TOCO is non-invasive but suffers from low resolution as it is sensitive to maternal motion artifacts [173]. EMG exhibits high

temporal resolution, but, due to the conductivity differences of tissue layers, results in attenuation of the recorded signal. Also, since EMG is recording the potential, results depend on the reference point which can produce only 2D views of the electrophysical activity. By contrast, MMG surpasses all approaches as (1) its operation is independent of tissue conductivity attenuation, (2) detection is non-invasive and non-contact and (3) may produce 3D mapping of localized sources.

IV. CONCLUSION

In this paper, we presented an overview of state-of-the-art and research-in-progress technologies used to detect human emitted bio-magnetic fields as well as their possible applications. In summary, detection of bio-magnetic fields is extremely challenging due to the low field strength and wide frequency bandwidth. Some of the most promising technologies entail SQUIDs, AMs, induction coil gradiometers, and shielding. Concurrently, future efforts should focus on (1) lowering the sensors' detection level; (2) improving noise performance; (3) increasing the shielding factor; (4) lowering the sensor cost, size, weight; (5) improving manufacturability; (6) enhancing safety; and (7) expanding the range of applications. Overall, detection of human emitted bio-magnetic signals opens up new opportunities for non-contact monitoring, diagnostics and prognostics in clinical healthcare settings and beyond.

ACKNOWLEDGMENT

The authors would like to thank Alden Joseph, Elizabeth Jergens, Gordon Weiss, and Daniel Wharton for preliminary literature review.

REFERENCES

[1] A. Hatano *et al.*, "CELLPEDIA: A repository for human cell information for cell studies and differentiation analyses," *Database*, vol. 2011, Oct. 2011, Art. no. bar046.

[2] D. Cohen, "Measurements of the magnetic fields produced by the human heart, brain, and lungs," *IEEE Trans. Magn.*, vol. MAG-11, no. 2, pp. 694–700, Mar. 1975.

[3] J. Haueisen *et al.*, "The influence of brain tissue anisotropy on human EEG and MEG," *NeuroImage*, vol. 15, no. 1, pp. 159–166, 2002.

[4] V. Mäntynen, T. Konttila, and M. Stenroos, "Investigations of sensitivity and resolution of ECG and MCG in a realistically shaped thorax model," *Phys. Med. Biol.*, vol. 59, no. 23, pp. 7141–7158, 2014.

[5] R. Pethig and D. B. Kell, "The passive electrical properties of biological systems: Their significance in physiology, biophysics and biotechnology," *Phys. Med. Biol.*, vol. 32, no. 8, pp. 933–970, 1987.

[6] G. Pei *et al.*, "Effects of an integrated neurofeedback system with dry electrodes: EEG acquisition and cognition assessment," *Sensors*, vol. 18, no. 10, p. 3396, 2018.

[7] V. S. Zotev *et al.*, "Multi-channel SQUID system for MEG and ultra-low-field MRI," *IEEE Trans. Appl. Supercond.*, vol. 17, no. 2, pp. 839–842, Jun. 2007.

[8] K. Zhu, A. M. Shah, J. Berkow, and A. Kiourti, "Miniature coil array for passive magnetocardiography in non-shielded environments," *IEEE J. Electromagn. RF Microw. Med. Biol.*, vol. 5, no. 2, pp. 124–131, Jun. 2021.

[9] A. Ziehe, K.-R. Muller, G. Nolte, B.-M. Mackert, and G. Curio, "Artifact reduction in magnetoneurography based on time-delayed second-order correlations," *IEEE Trans. Biomed. Eng.*, vol. 47, no. 1, pp. 75–87, Jan. 2000.

[10] Y. Adachi, D. Oyama, J. Kawai, S. Kawabata, and G. Uehara, "Spinal cord evoked magnetic field measurement using a magnetospinography system equipped with a cryocooler," in *Proc. 35th Annu. Int. Conf. IEEE Eng. Med. Biol. Soc. (EMBC)*, 2013, pp. 4426–4429.

[11] D. Escalona-Vargas, E. R. Siegel, S. Oliphant, and H. Eswaran, "Evaluation of pelvic floor muscles in pregnancy and postpartum with non-invasive magnetomyography," *IEEE J. Transl. Eng. Health Med.*, vol. 10, pp. 1–6, 2022.

[12] K. Kobayashi, M. Yoshizawa, D. Oyama, and Y. Uchikawa, "Wide dynamic range analog flux-locked loop system using low-Tc SQUID for MCG measurements without MSR," *IEEE Trans. Magn.*, vol. 50, no. 11, pp. 1–3, Nov. 2014.

[13] S. Sinha, P. Satishchandra, and J. Velmurugan, "Magnetoencephalography recording and analysis," *Ann. Indian Acad. Neurol.*, vol. 17, no. 5, p. 113, 2014.

[14] P. P. Swain, S. Sengottuvel, R. Patel, A. Mani, and K. Gireesan, "A feasibility study to measure magnetocardiography (MCG) in unshielded environment using first order gradiometer," *Biomed. Signal Process. Control*, vol. 55, Jan. 2020, Art. no. 101664.

[15] Y. Adachi, D. Oyama, N. Somchai, S. Kawabata, and G. Uehara, "Simplified spinal cord phantom for evaluation of squid magnetospinography," *J. Phys. Conf. Series*, vol. 507, no. 4, 2014, Art. no. 042001.

[16] H. Heidari, S. Zuo, A. Krasoulis, and K. Nazarpour, "CMOS magnetic sensors for wearable magnetomyography," in *Proc. 40th Annu. Int. Conf. IEEE Eng. Med. Biol. Soc. (EMBC)*, 2018, pp. 2116–2119.

[17] B.-M. Mackert, "Magnetoneurography: Theory and application to peripheral nerve disorders," *Clin. Neurophysiol.*, vol. 115, no. 12, pp. 2667–2676, 2004.

[18] S. Zuo, H. Heidari, D. Farina, and K. Nazarpour, "Miniaturized magnetic sensors for implantable magnetomyography," *Adv. Mater. Technol.*, vol. 5, no. 6, 2020, Art. no. 2000185.

[19] D. Escalona-Vargas, S. Oliphant, E. R. Siegel, and H. Eswaran, "Characterizing pelvic floor muscles activities using magnetomyography," *Neurourol. Urodyn.*, vol. 38, no. 1, pp. 151–157, 2018.

[20] H. Eswaran, H. Preissl, J. D. Wilson, P. Murphy, and C. L. Lowery, "Prediction of labor in term and preterm pregnancies using non-invasive magnetomyographic recordings of uterine contractions," *Amer. J. Obstetrics Gynecol.*, vol. 190, no. 6, pp. 1598–1602, 2004.

[21] D. Cohen, "Magnetoencephalography: Evidence of magnetic fields produced by alpha-rhythm currents," *Science*, vol. 161, no. 3843, pp. 784–786, 1968.

[22] G. M. Baule and R. McFee, "The magnetic heart vector," *Amer. Heart J.*, vol. 79, no. 2, pp. 223–236, 1970.

[23] K. Guido, A. Clavijao, K. Zhu, X. Ding, and K. Ma, "Strategies to improve neural electrode performance," in *Neural Interface Engineering*. Cham, Switzerland: Springer, May 2020, pp. 173–199.

[24] K. Gramm, L. Lundgren, and O. Beckman, "Squid magnetometer for mangetization measurements," *Physica Scripta*, vol. 13, no. 2, pp. 93–95, 1976.

[25] J. R. Claycomb and J. H. Miller, "Superconducting magnetic shields for SQUID applications," *Rev. Sci. Instrum.*, vol. 70, no. 12, pp. 4562–4568, 1999.

[26] M. I. Faley *et al.*, "High-Tc SQUID biomagnetometers," *Supercond. Sci. Technol.*, vol. 30, no. 8, 2017, Art. no. 083001.

[27] K. Kobayashi, Y. Uchikawa, K. Nakai, and M. Yoshizawa, "Analysis and estimation of excitation conduction with Wolff–Parkinson–White syndrome patients based on a 3-D magnetocardiogram," *IEEE Trans. Magn.*, vol. 38, no. 5, pp. 3338–3340, Sep. 2002.

[28] Elekta. "Elekta AB." Jan. 2020. [Online]. Available: https://www.elekta.com/meta/press-intern/?id=c9c8fa2c-349a-4835-bd8b-78231ec2729c

[29] M. Faley, E. Kostyurina, K. Kalashnikov, Y. Maslennikov, V. Koshelets, and R. Dunin-Borkowski, "Superconducting quantum interferometers for nondestructive evaluation," *Sensors*, vol. 17, no. 12, p. 2798, 2017.

[30] H. J. M. ter Brake *et al.*, "Fetal magnetocardiography: Clinical relevance and feasibility," *Physica C Supercond.*, vol. 368, nos. 1–4, pp. 10–17, 2002.

[31] T. Uchiyama and T. Takiya, "Development of precise off-diagonal magnetoimpedance gradiometer for magnetocardiography," *AIP Adv.*, vol. 7, no. 5, 2017, Art. no. 056644.

[32] D. Karnaushenko, D. D. Karnaushenko, D. Makarov, S. Baunack, R. Schäfer, and O. G. Schmidt, "Self-assembled on-chip-integrated giant magneto-impedance sensorics," *Adv. Mater.*, vol. 27, no. 42, pp. 6582–6589, 2015.

[33] T. Takiya and T. Uchiyama, "Development of an active shielding-type MI gradiometer: Its application for Magnetocardiography," in *Proc. IEEE Int. Magn. Conf. (INTERMAG)*, 2017, pp. 1–8.

[34] P. J. Broser *et al.*, "Optically pumped magnetometers for Magneto-myography to study the innervation of the hand," *IEEE Trans. Neural Syst. Rehabil. Eng.*, vol. 26, no. 11, pp. 2226–2230, Nov. 2018.

[35] C. Pfeiffer *et al.*, "A 7-channel high-Tc SQUID-based on-scalp MEG system," *IEEE Trans. Biomed. Eng.*, vol. 67, no. 5, pp. 1483–1489, May 2020.

[36] L. M. Andersen *et al.*, "On-scalp MEG SQUIDs are sensitive to early somatosensory activity unseen by conventional MEG," *NeuroImage*, vol. 221, Nov. 2020, Art. no. 117157.

[37] S. Morales *et al.*, "Magnetocardiography measurements with ^{4}He vector optically pumped magnetometers at room temperature," *Phys. Med. Biol.*, vol. 62, no. 18, pp. 7267–7279, 2017.

[38] Y. V. Maslennikov, "Magnetocardiographic diagnostic complexes based on the MAG-SKAN squids," *J. Commun. Technol. Electron.*, vol. 56, no. 8, pp. 991–999, 2011.

[39] Y. V. Maslennikov *et al.*, "The DC-SQUID-based magnetocardiographic systems for clinical use," *Phys. Procedia*, vol. 36, pp. 88–93, Sep. 2012.

[40] J. W. Mooney *et al.*, "A portable diagnostic device for cardiac magnetic field mapping," *Biomed. Phys. Eng. Exp.*, vol. 3, no. 1, 2017, Art. no. 015008.

[41] J. Belfi, G. Bevilacqua, V. Biancalana, S. Cartaleva, Y. Dancheva, and L. Moi, "Cesium coherent population trapping magnetometer for cardiosignal detection in an unshielded environment," *J. Opt. Soc. Amer. B*, vol. 24, no. 9, p. 2357, 2007.

[42] R. Zhang *et al.*, "Recording brain activities in unshielded Earth's field with optically pumped atomic magnetometers," *Sci. Adv.*, vol. 6, no. 24, 2020, Art. no. aba8792.

[43] C. Deans, L. Marmugi, and F. Renzoni, "Sub-picotesla widely tunable atomic magnetometer operating at room-temperature in unshielded environments," *Rev. Sci. Instrum.*, vol. 89, no. 8, 2018, Art. no. 083111.

[44] S. Baillet, "Magnetoencephalography for brain electrophysiology and imaging," *Nat. Neurosci.*, vol. 20, no. 3, pp. 327–339, 2017.

[45] R. Körber *et al.*, "Squids in biomagnetism: A roadmap towards improved healthcare," *Supercond. Sci. Technol.*, vol. 29, no. 11, 2016, Art. no. 113001.

[46] Z. Gao, H. Dang, D. Bao, and Y. Zhao, "Investigation on a three-stage stirling-type pulse tube cryocooler for cooling the low-Tc SQUID," *IEEE Trans. Appl. Supercond.*, vol. 27, no. 4, pp. 1–5, Jun. 2017.

[47] F. Öisjöen *et al.*, "High-TC superconducting quantum interference device recordings of spontaneous brain activity: Towards high-TC magnetoencephalography," *Appl. Phys. Lett.*, vol. 100, no. 13, 2012, Art. no. 132601.

[48] J. Clarke, Y.-H. Lee, and J. Schneiderman, "Focus on squids in biomagnetism," *Supercond. Sci. Technol.*, vol. 31, no. 8, 2018, Art. no. 080201.

[49] J. Kawai, M. Miyamoto, M. Kawabata, and G. Uehara, "Improvement of performance of SQUID magnetometer system for highly sensitive geomagnetic field measurements," *IEEE Trans. Appl. Supercond.*, vol. 28, no. 8, pp. 1–7, Dec. 2018.

[50] C. S. Kang *et al.*, "Measurement of MCG in unshielded environment using a second-order SQUID gradiometer," *IEEE Trans. Magn.*, vol. 45, no. 6, pp. 2882–2885, Jun. 2009.

[51] Y. Zhang *et al.*, "HTS squid gradiometer using substrate resonators operating in an unshielded environment—A portable MCG system," *IEEE Trans. Appl. Supercond.*, vol. 13, no. 2, pp. 389–392, Jun. 2003.

[52] M. I. Faley *et al.*, "High-Tc DC SQUIDs for magnetoencephalography," *IEEE Trans. Appl. Supercond.*, vol. 23, no. 3, Jun. 2013, Art. no. 1600705.

[53] M. I. Faley *et al.*, "Magnetoencephalography using a multilayer hightc DC Squid magnetometer," *Phys. Procedia*, vol. 36, pp. 66–71, Sep. 2012.

[54] H. Eswaran, H. Preissl, J. D. Wilson, P. Murphy, S. E. Robinson, and C. L. Lowery, "First magnetomyographic recordings of uterine activity with spatial–temporal information with a 151-channel sensor array," *Amer. J. Obstetrics Gynecol.*, vol. 187, no. 1, pp. 145–151, 2002.

[55] A. Klein, P. van Leeuwen, J. Hoormann, and D. Grönemeyer, "Magnetoneurographic registration of propagating magnetic fields in the lumbar spine after stimulation of the posterior tibial nerve," *J. Neural Eng.*, vol. 3, no. 2, pp. 125–131, 2006.

[56] Y. Adachi *et al.*, "Improvement of squid magnetometer system for extending application of spinal cord evoked magnetic field measurement," *IEEE Trans. Appl. Supercond.*, vol. 21, no. 3, pp. 485–488, Jun. 2011.

[57] Y. Adachi, J. Kawai, G. Uehara, M. Miyamoto, S. Tomizawa, and S. Kawabata, "A 75-ch SQUID Biomagnetometer system for human cervical spinal cord evoked field," *IEEE Trans. Appl. Supercond.*, vol. 17, no. 4, pp. 3867–3873, Dec. 2007.

[58] H. Ohta, T. Matsui, and Y. Uchikawa, "Studies on response of human hippocampus to random somatosensory stimuli by a squid system in a superconducting magnetic shield," *IEEE Trans. Appl. Supercond.*, vol. 21, no. 3, pp. 469–472, Jun. 2011.

[59] V. Pizzella, S. D. Penna, C. D. Gratta, and G. L. Romani, "SQUID systems for biomagnetic imaging," *Supercond. Sci. Technol.*, vol. 14, no. 7, p. R79, 2001.

[60] T. Matsumoto, H. Kashiwaya, H. Shibata, H. Takayanagi, S. Nomura, and S. Kashiwaya, "Fabrication of weak-link Nb-based nano-SQUIDs by FIB process," *Physica C Supercond. Appl.*, vol. 471, nos. 21–22, pp. 1246–1248, 2011.

[61] C. H. Wu *et al.*, "Fabrication and characterization of high-Tc YBa2Cu3O7−x nanoSQUIDs made by focused ion beam milling," *Nanotechnology*, vol. 19, no. 31, 2008, Art. no. 315304.

[62] D. Dimos, P. Chaudhari, J. Mannhart, and F. K. LeGoues, "Orientation dependence of grain-boundary critical currents in $YBa_2Cu_3O_7$-bicrystals," *Phys. Rev. Lett.*, vol. 61, no. 2, pp. 219–222, 1988.

[63] J. Mmurduck, "Fabrication of superconducting devices and circuits," in *Handbook of Thin Film Devices*. San Diego, CA, USA: Academic, 2000, pp. 35–69.

[64] H. Li, E. Y. Cho, H. Cai, Y.-T. Wang, S. J. McCoy, and S. A. Cybart, "Inductance investigation of YBa2Cu3O7−δ nano-slit SQUIDs fabricated with a focused helium ion beam," *IEEE Trans. Appl. Supercond.*, vol. 29, no. 5, pp. 1–4, Aug. 2019.

[65] F. Ludwig *et al.*, "Low noise $YBa_2Cu_3O_7$-x-$SrTiO_3$-$YBa_2Cu_3O_7$-x multilayers for improved superconducting magnetometers," *Appl. Phys. Lett.*, vol. 66, no. 3, pp. 373–375, 1995.

[66] J. Sheng *et al.*, "Magnetoencephalography with a CS-based high-sensitivity compact atomic magnetometer," *Rev. Sci. Instrum.*, vol. 88, no. 9, 2017, Art. no. 094304.

[67] J. Li *et al.*, "SERF atomic magnetometer-recent advances and applications: A review," *IEEE Sensors J.*, vol. 18, no. 20, pp. 8198–8207, Oct. 2018.

[68] D. Budker and M. Romalis, "Optical magnetometry," *Nat. Phys.*, vol. 3, no. 4, pp. 227–234, 2007.

[69] O. Alem *et al.*, "Fetal magnetocardiography measurements with an array of microfabricated optically pumped magnetometers," *Phys. Med. Biol.*, vol. 60, no. 12, pp. 4797–4811, 2015.

[70] K. Kamada, Y. Ito, and T. Kobayashi, "Human MCG measurements with a high-sensitivity potassium atomic magnetometer," *Physiol. Meas.*, vol. 33, no. 6, pp. 1063–1071, 2012.

[71] J. Iivanainen, R. Zetter, M. Grön, K. Hakkarainen, and L. Parkkonen, "On-scalp MEG system utilizing an actively shielded array of optically-pumped magnetometers," *NeuroImage*, vol. 194, pp. 244–258, Jul. 2019.

[72] K. Nishi, Y. Ito, and T. Kobayashi, "High-sensitivity multi-channel probe beam detector towards MEG measurements of small animals with an optically pumped K-RB hybrid magnetometer," *Opt. Exp.*, vol. 26, no. 2, p. 1988, 2018.

[73] H. Xia, A. B.-A. Baranga, D. Hoffman, and M. V. Romalis, "Magnetoencephalography with an atomic magnetometer," *Appl. Phys. Lett.*, vol. 89, no. 21, 2006, Art. no. 211104.

[74] J.-J. Li, P.-C. Du, J.-Q. Fu, X.-T. Wang, Q. Zhou, and R.-Q. Wang, "Miniature quad-channel spin-exchange relaxation-free magnetometer for magnetoencephalography," *Chin. Phys. B*, vol. 28, no. 4, 2019, Art. no. 040703.

[75] G. Zhang, S. Huang, F. Xu, Z. Hu, and Q. Lin, "Multi-channel spin exchange relaxation free magnetometer towards two-dimensional vector magnetoencephalography," *Opt. Exp.*, vol. 27, no. 2, p. 597, 2019.

[76] K. Kamada *et al.*, "Human magnetoencephalogram measurements using newly developed compact module of high-sensitivity atomic magnetometer," *Jpn. J. Appl. Phys.*, vol. 54, no. 2, 2015, Art. no. 026601.

[77] V. Shah, J. Osborne, J. Orton, and O. Alem, "Fully integrated, standalone zero field optically pumped magnetometer for biomagnetism," in *Proc. Steep Dispersion Eng. Opto-Atom. Precision Metrol. XI*, 2018, Art. no. 105481G.

[78] V. K. Shah and R. T. Wakai, "A compact, high performance atomic magnetometer for biomedical applications," *Phys. Med. Biol.*, vol. 58, no. 22, pp. 8153–8161, 2013.

[79] G. Z. Iwata *et al.*, "Biomagnetic signals recorded during transcranial magnetic stimulation (TMS)-evoked peripheral muscular activity," 2019, *arXiv:1909.11451*.

[80] P. Broser, T. Middelmann, D. Sometti, and C. Braun, "Optically pumped magnetometers disclose magnetic field components of the muscular action potential," *J. Electromyography Kinesiol.*, vol. 56, Feb. 2021, Art. no. 102490.

[81] E. Elzenheimer, H. Laufs, W. Schulte-Mattler, and G. Schmidt, "Magnetic measurement of electrically evoked muscle responses with optically pumped magnetometers," *IEEE Trans. Neural Syst. Rehabil. Eng.*, vol. 28, no. 3, pp. 756–765, Mar. 2020.

[82] J. F. Schneiderman, "Information content with low- vs. high-TC squid arrays in MEG recordings: The case for high-TC squid-based MEG," *J. Neurosci. Methods*, vol. 222, pp. 42–46, Jan. 2014.

[83] J. C. Allred, R. N. Lyman, T. W. Kornack, and M. V. Romalis, "High-sensitivity atomic magnetometer unaffected by spin-exchange relaxation," *Phys. Rev. Lett.*, vol. 89, no. 13, 2002, Art. no. 130801.

[84] S. Strand, W. Lutter, J. F. Strasburger, V. Shah, O. Baffa, and R. T. Wakai, "Low-cost fetal magnetocardiography: A comparison of superconducting quantum interference device and optically pumped magnetometers," *J. Amer. Heart Assoc.*, vol. 8, no. 16, 2019, Art. no. e013436.

[85] N. An *et al.*, "Multiple source detection based on spatial clustering and its applications on wearable OPM-MEG," *IEEE Trans. Biomed. Eng.*, early access, Mar. 23, 2022, doi: 10.1109/TBME.2022.3161830.

[86] J. Zhang, K. Liu, J. Zhang, Z. Wang, and J. Shang, "Magnetocardiography measurements by microfabricated atomic magnetometer with a 3-D spherical alkali vapor cell," *IEEE Trans. Instrum. Meas.*, vol. 70, pp. 1–7, 2021.

[87] K. Tashiro, "Induction coil magnetometers," *Smart Sensors Meas. Instrum.*, vol. 19, pp. 1–39, Sep. 2016.

[88] K. Tashiro, "Optimal design of an air-core induction magnetometer for detecting low-frequency fields of less than 1 PT," *J. Magn. Soc. Japan*, vol. 30, no. 4, pp. 439–442, 2006.

[89] S. Celozzi and G. Lovat, "Appendix B: Magnetic shielding," in *Electromagnetic Shielding*, R. Araneo, Ed. Hoboken, NJ, USA: Wiley, 2008, pp. 282–316.

[90] Y. C. Okada, B. Shah, and J.-C. Huang, "Ferromagnetic high-permeability alloy alone can provide sufficient low-frequency and eddy-current shieldings for biomagnetic measurements," *IEEE Trans. Biomed. Eng.*, vol. 41, no. 7, pp. 688–697, Jul. 1994.

[91] D. Platzek, H. Nowak, F. Giessler, J. Röther, and M. Eiselt, "Active shielding to reduce low frequency disturbances in direct current near biomagnetic measurements," *Rev. Sci. Instrum.*, vol. 70, no. 5, pp. 2465–2470, 1999.

[92] B. Hilgenfeld, E. Str hmel, H. Nowak, and J. Haueisen, "Active magnetic shielding for biomagnetic measurement using spatial gradient fields," *Physiol. Meas.*, vol. 24, no. 3, pp. 661–669, 2003.

[93] V. Kelha, J. Pukki, R. Peltonen, A. Penttinen, R. Ilmoniemi, and J. Heino, "Design, construction, and performance of a large-volume magnetic shield," *IEEE Trans. Magn.*, vol. MAG-18, no. 1, pp. 260–270, Jan. 1982.

[94] P. J. Hobson *et al.*, "Optimised hybrid shielding and magnetic field control for emerging quantum technologies," in *Proc. Quant. Technol. Driving Commercialisation Enabling Sci. II*, 2021, Art. no. 1188110.

[95] L. Hasselgren and J. Luomi, "Geometrical aspects of magnetic shielding at extremely low frequencies," *IEEE Trans. Electromagn. Compat.*, vol. 37, no. 3, pp. 409–420, Aug. 1995.

[96] M. Sakakibara, G. Uehara, and Y. Adachi, "Prediction of cylindrical magnetic shielding performance by considering the magnetic field strength inside the material," *IEEE Trans. Magn.*, vol. 58, no. 2, pp. 1–4, Feb. 2022.

[97] M. Sakakibara, G. Uehara, Y. Adachi, and T. Meguro, "Evaluation of heat treatment of MU-metal based on permeability under very-low-frequency micromagnetic fields," *IEEE Trans. Mag.*, vol. 57, no. 2, pp. 1–4, Feb. 2021.

[98] T. W. Kornack, S. J. Smullin, S.-K. Lee, and M. V. Romalis, "A low-noise ferrite magnetic shield," *Appl. Phys. Lett.*, vol. 90, no. 22, 2007, Art. no. 223501.

[99] S. Yamada and I. Yamaguchi, "Magnetocardiograms in clinical medicine: Unique information on cardiac ischemia, arrhythmias, and fetal diagnosis," *Int. Med.*, vol. 44, no. 1, pp. 1–19, 2005.

[100] R. Fenici, D. Brisinda, and A. M. Meloni, "Clinical application of magnetocardiography," *Exp. Rev. Mol. Diagn.*, vol. 5, no. 3, pp. 291–313, 2005.

[101] E. A. P. Alday, C. Zhang, M. A. Colman, H. Ni, Z. Gan, and H. Zhang, "Comparison of electric- and magnetic- cardiograms produced by myocardial ischemia in models of the human ventricle and torso," in *Proc. Comput. Cardiol. Conf. (CinC)*, 2015, pp. 517–520.

[102] F. E. Smith *et al.*, "Comparison of magnetocardiography and electrocardiography: A study of automatic measurement of dispersion of ventricular repolarization," *EP Europace*, vol. 8, no. 10, pp. 887–893, 2006.

[103] B. Hailer and P. V. Leeuwen, "Detection of coronary artery disease with MCG," *Neurol. Clin. Neurophysiol.*, vol. 30, p. 82, Nov. 2004.

[104] About Heart Disease. "Centers for Disease Control and Prevention." Sep. 27, 2021. [Online]. Available: https://www.cdc.gov/heartdisease/about.htm (Accessed: May 9, 2022).

[105] J.-P. Collet *et al.*, "2020 ESC guidelines for the management of acute coronary syndromes in patients presenting without persistent ST-segment elevation," *Eur. Heart J.*, vol. 42, no. 14, pp. 1289–1367, 2020.

[106] D. Cohen, J. C. Norman, F. Molokhia, and W. Hood, "Magnetocardiography of direct currents: S-T segment and baseline shifts during experimental myocardial infarction," *Science*, vol. 172, no. 3990, pp. 1329–1333, 1971.

[107] J.-W. Park, P. M. Hill, N. Chung, P. G. Hugenholtz, and F. Jung, "Magnetocardiography predicts coronary artery disease in patients with acute chest pain," *Ann. Noninvasive Electrocardiol.*, vol. 10, no. 3, pp. 312–323, 2005.

[108] R. Tao *et al.*, "Magnetocardiography-based ischemic heart disease detection and localization using machine learning methods," *IEEE Trans. Biomed. Eng.*, vol. 66, no. 6, pp. 1658–1667, Jun. 2019.

[109] J. Nenonen and B. Nenonen, "Simulation of extracardiac electromagnetic field due to propagated excitation in the anisotropic ventricular myocardium," in *Biomedical and Life Physics*, D. Ghista, Ed. Berlin, Germany: Viewer Verlag, 1996, pp. 191–202.

[110] P. Weismuller *et al.*, "Spatial differences of the duration of ventricular late fields in the signal-averaged magnetocardiogram in patients with ventricular late potentials," *Pacing Clin. Electrophysiol.*, vol. 16, no. 1, pp. 70–79, 1993.

[111] P. Kochonen, J. Mointonen, M. Makinarvi, T. Katila, M. S. Nieminen, and L. Toivonen, "Late fields of the magnetocardiographic QRS complex as indicators of propensity to sustained ventricular tachycardia after myocardial infarction," *J. Cardiovascul. Electrophysiol.*, vol. 11, no. 4, pp. 413–420, 2000.

[112] V. Kariniemi, J. Ahopelto, P. J. Karpi, and T. E. Katila, "The fetal magnetocardiogram," *J. Perinatal Med.*, vol. 2, no. 3, pp. 214–216, 1974.

[113] T. Menéndez *et al.*, "Pränatale registrierung fetaler herzaktionen mit magnetokardiographie," *Zeitschrift fur Kardiologie*, vol. 87, no. 2, pp. 111–118, 1998.

[114] H. Horigome, M. I. Takahashi, M. Asaka, S. Shigemitsu, A. Kandori, and K. Tsukada, "Magnetocardiographic determination of the developmental changes in PQ, QRS and qt intervals in the foetus," *Acta Paediatrica*, vol. 89, no. 1, pp. 64–67, 2007.

[115] P. T. Tang, M. Shenasa, and N. G. Boyle, "Ventricular arrhythmias and sudden cardiac death," *Cardiac Electrophysiol. Clinics*, vol. 9, no. 4, pp. 693–708, 2017.

[116] P. Korhonen *et al.*, "Increased intra-QRS fragmentation in magnetocardiography as a predictor of arrhythmic events and mortality in patients with cardiac dysfunction after myocardial infarction," *J. Cardiovascul. Electrophysiol.*, vol. 17, no. 4, pp. 396–401, 2006.

[117] B. Hailer and P. Leeuwen, "Prediction of malignant arrhythmias after myocardial infarction on the basis of MCG," in *Proc. 12th Int. Conf. Biomagnetism*, vol. 504, 2001, pp. 1–9.

[118] J. Mayet *et al.*, "Left ventricular hypertrophy and QT dispersion in hypertension," *Hypertension*, vol. 28, no. 5, pp. 791–796, 1996.

[119] N. Iwakami *et al.*, "Identification of malignant early repolarization pattern by late QRS activity in high-resolution magnetocardiography," *Ann. Noninvasive Electrocardiol.*, vol. 25, no. 4, 2020, Art. no. e12741.

[120] H.-P. Müller *et al.*, "Magnetocardiographic analysis of the two-dimensional distribution of intra-QRS fractionated activation," *Phys. Med. Biol.*, vol. 44, no. 1, pp. 105–120, 1999.

[121] P. Endt *et al.*, "Identification of post-myocardial infarction patients with ventricular tachycardia by time-domain intra-QRS analysis of signal-averaged electrocardiogram and magnetocardiogram," *Med. Biol. Eng. Comput.*, vol. 38, no. 6, pp. 659–665, 2000.

[122] P. Korhonen *et al.*, "Magnetocardiographic intra-qrs fragmentation analysis in the identification of patients with sustained ventricular tachycardia after myocardial infarction," *Pacing Clin. Electrophysiol.*, vol. 24, no. 8, pp. 1179–1186, 2001.

[123] A.-Y. Her and J.-W. Park, "Repolarization heterogeneity of magnetocardiography predicts long-term prognosis in patients with acute myocardial infarction," *Yonsei Med. J.*, vol. 57, no. 6, p. 1305, 2016.

[124] D. Fernando and J. Resar, "Magnetocardiography in cardiac transplantation: A case study," *Int. J. Bioelectromagn.*, vol. 5, no. 1, pp. 109–113, 2003.

[125] R. R. Fenici, G. Melillo, and M. Masselli, "Clinical magnetocardiography," *Int. J. Cardiac Imag.*, vol. 7, nos. 3–4, pp. 151–167, 1991.

[126] I. Tavarozzi *et al.*, "Magnetocardiography: Current status and perspectives. Part II: Clinical applications," *Italian Heart J.*, vol. 3, no. 3, pp. 151–165, 2002.

[127] T. Hosono, K. Kawamata, Y. Chiba, A. Kandori, and K. Tsukada, "Prenatal diagnosis of long QT syndrome using magnetocardiography: A case report and review of the literature," *Prenatal Diagn.*, vol. 22, no. 3, pp. 198–200, 2002.

[128] T. Hosono, Y. Chiba, M. Shinto, A. Kandori, and K. Tsukada, "A fetal Wolff–Parkinson–White syndrome diagnosed prenatally by magnetocardiography," *Fetal Diagn. Therapy*, vol. 16, no. 4, pp. 215–217, 2001.

[129] A. Quinn, A. Weir, U. Shahani, R. Bain, P. Maas, and G. Donaldson, "Antenatal fetal magnetocardiography: A new method for fetal surveillance?" *Int. J. Obstetrics Gynaecol.*, vol. 101, no. 10, pp. 866–870, 1994.

[130] T. Hosono *et al.*, "A case of fetal complete heart block recorded by magnetocardiography, ultrasonography and direct fetal electrocardiography," *Fetal Diagn. Therapy*, vol. 16, no. 1, pp. 38–41, 2000.

[131] M. Balish, S. Sato, P. Connaughton, and C. Kufta, "Localization of implanted dipoles by magnetoencephalography," *Neurology*, vol. 41, no. 7, pp. 1072–1072, 1991.

[132] M. Oishi *et al.*, "Epileptic spikes: Magnetoencephalography versus simultaneous electrocorticography," *Epilepsia*, vol. 43, no. 11, pp. 1390–1395, 2002.

[133] R. C. Knowlton, K. D. Laxer, M. J. Aminoff, T. P. Roberts, S. T. Wong, and H. A. Rowley, "Magnetoencephalography in partial epilepsy: Clinical yield and localization accuracy," *Ann. Neurol.*, vol. 42, no. 4, pp. 622–631, 1997.

[134] C. Baumgartner, E. Pataraia, G. Lindinger, and L. Deecke, "Neuromagnetic recordings in temporal lobe epilepsy," *J. Clin. Neurophysiol.*, vol. 17, no. 2, pp. 177–189, 2000.

[135] N. Mikuni *et al.*, "Simultaneous recording of epileptiform discharges by MEG and subdural electrodes in temporal lobe epilepsy," *NeuroImage*, vol. 5, no. 4, pp. 298–306, 1997.

[136] P. Ossenblok, J. C. de Munck, A. Colon, W. Drolsbach, and P. Boon, "Magnetoencephalography is more successful for screening and localizing frontal lobe epilepsy than electroencephalography," *Epilepsia*, vol. 48, no. 11, pp. 2139–2149, 2007.

[137] E. Schleussner, U. Schneider, S. Kausch, C. Kähler, J. Haueisen, and H.-J. Seewald, "Fetal magnetoencephalography: A non-invasive method for the assessment of fetal neuronal maturation," *Brit. J. Obstetrics Gynaecol.*, vol. 108, no. 12, pp. 1291–1294, 2001.

[138] H. Eswaran, C. L. Lowery, J. D. Wilson, P. Murphy, and H. Preissl, "Functional development of the visual system in human fetus using magnetoencephalography," *Exp. Neurol.*, vol. 190, no. S1, pp. 52–58, 2004.

[139] C. J. Sheridan, T. Matuz, R. Draganova, H. Eswaran, and H. Preissl, "Fetal magnetoencephalography-achievements and challenges in the study of prenatal and early postnatal brain responses: A review," *Infant Child Develop.*, vol. 19, no. 1, pp. 80–93, 2010.

[140] J. O. Davidson, J. S. Quaedackers, S. A. George, A. J. Gunn, and L. Bennet, "Maternal dexamethasone and EEG hyperactivity in preterm fetal sheep," *J. Physiol.*, vol. 589, no. 15, pp. 3823–3835, 2011.

[141] A. A. Benasich and P. Tallal, "Infant discrimination of rapid auditory cues predicts later language impairment," *Behav. Brain Res.*, vol. 136, no. 1, pp. 31–49, 2002.

[142] A. I. Bagić, R. C. Knowlton, D. F. Rose, and J. S. Ebersole, "American clinical magnetoencephalography society clinical practice guideline 1," *J. Clin. Neurophysiol.*, vol. 28, no. 4, pp. 348–354, 2011.

[143] S. P. Singh, "Magnetoencephalography: Basic principles," *Ann. Indian Acad. Neurol.*, vol. 17, no. 5, p. 107, 2014.

[144] E. M. P. Knight, J. Gonzalez-Martinez, and A. Gupta, "Pre-operative evaluation in pediatric patients with cortical dysplasia," *Child Nervous Syst.*, vol. 31, no. 12, pp. 2225–2233, 2015.

[145] A. Blenkmann, G. Seifer, J. P. Princich, D. Consalvo, S. Kochen, and C. Muravchik, "Association between equivalent current dipole source localization and focal cortical dysplasia in epilepsy patients," *Epilepsy Res.*, vol. 98, nos. 2–3, pp. 223–231, 2012.

[146] M. J. Fischer, "Utilization of magnetoencephalography results to obtain favourable outcomes in epilepsy surgery," *Brain*, vol. 128, no. 1, pp. 153–157, 2004.

[147] S. Vadera *et al.*, "Correlation between magnetoencephalography-based 'clusterectomy' and postoperative seizure freedom," *Neurosurg. Focus*, vol. 34, no. 6, p. E9, 2013.

[148] P. Jayakar, W. D. Gaillard, M. Tripathi, M. H. Libenson, G. W. Mathern, and J. H. Cross, "Diagnostic test utilization in evaluation for resective epilepsy surgery in children," *Epilepsia*, vol. 55, no. 4, pp. 507–518, 2014.

[149] F. H. da Lopes Silva, "What is magnetoencephalography and why it is relevant to neurosurgery?" in *Advances and Technical Standards in Neurosurgery*, vol. 30. Vienna, Austria: Springer, 2005, pp. 51–67.

[150] S. Collinge *et al.*, "Pre-surgical mapping of eloquent cortex for paediatric epilepsy surgery candidates: Evidence from a review of advanced functional neuroimaging," *Seizure*, vol. 52, pp. 136–146, Nov. 2017.

[151] M. W. Watkins *et al.*, "Indications for inpatient magnetoencephalography in children—An institution's experience," *Front. Human Neurosci.*, vol. 15, Jun. 2021, Art. no. 667777.

[152] A. Keil, "Electro-and magnetoencephalography in the study of emotion," in *The Cambridge Handbook of Human Affective Neuroscience*, J. Armony and P. Vuilleumier, Eds. Cambridge, U.K.: Cambridge Univ. Press, 2013, pp. 132–137.

[153] K. Domschke *et al.*, "Magnetoencephalographic correlates of emotional processing in major depression before and after pharmacological treatment," *Int. J. Neuropsychopharmacol.*, vol. 19, no. 2, 2015, Art. no. pyv093.

[154] Y. Cheng, C.-Y. Yang, C.-P. Lin, P.-L. Lee, and J. Decety, "The perception of pain in others suppresses somatosensory oscillations: A magnetoencephalography study," *NeuroImage*, vol. 40, no. 4, pp. 1833–1840, 2008.

[155] F. A. Maratos, K. Mogg, B. P. Bradley, G. Rippon, and C. Senior, "Coarse threat images reveal theta oscillations in the amygdala: A magnetoencephalography study," *Cogn. Affective Behav. Neurosci.*, vol. 9, no. 2, pp. 133–143, 2009.

[156] Y. Yokota and Y. Naruse, "Phase coherence of auditory steady-state response reflects the amount of cognitive workload in a modified N-back task," *Neurosci. Res.*, vol. 100, pp. 39–45, Nov. 2015.

[157] W. McClay, N. Yadav, Y. Ozbek, A. Haas, H. Attias, and S. Nagarajan, "A real-time magnetoencephalography brain–computer interface using interactive 3D visualization and the Hadoop ecosystem," *Brain Sci.*, vol. 5, no. 4, pp. 419–440, 2015.
[158] L. Kauhanen *et al.*, "EEG and MEG brain–computer interface for tetraplegic patients," *IEEE Trans. Neural Syst. Rehabil. Eng.*, vol. 14, no. 2, pp. 190–193, Jun. 2006.
[159] S. Ushio *et al.*, "Visualization of the electrical activity of the cauda equina using a magnetospinography system in healthy subjects," *Clin. Neurophysiol.*, vol. 130, no. 1, pp. 1–11, 2019.
[160] K. Sakaki *et al.*, "Evaluation of neural activity by magnetospinography with 3D sensors," *Clin. Neurophysiol.*, vol. 131, no. 6, pp. 1252–1266, 2020.
[161] S. Kawabata *et al.*, "Diagnosis of conduction block in cervical myelopathy patients by non-invasive magnetospinography," *J. Neurol. Sci.*, vol. 405, no. 1, pp. 33–34, 2019.
[162] S. Kawabata *et al.*, "Evaluation of spinal conduction block in myelopaty patients by magnetospinography," *J. Neurol. Sci.*, vol. 381, p. 801, Oct. 2017.
[163] S. Sumiya *et al.*, "Magnetospinography visualizes electrophysiological activity in the cervical spinal cord," *Sci. Rep.*, vol. 7, no. 1, p. 2192, 2017.
[164] Y. Miyano *et al.*, "Visualization of electrical activity in the cervical spinal cord and nerve roots after ulnar nerve stimulation using magnetospinography," *Clin. Neurophysiol.*, vol. 131, no. 10, pp. 2460–2468, 2020.
[165] M. Akaza *et al.*, "T108. magnetic recordings of sensory action currents in the cervical cord," *Clin. Neurophysiol.*, vol. 129, no. 1, p. e44, 2018.
[166] T. Watanabe *et al.*, "T110. visualization of nerve impulse traveling along the brachial plexus after ulnar nerve stimulation using magnetoneurography system," *Clin. Neurophysiol.*, vol. 129, no. 1, pp. e44–e45, 2018.
[167] S. Kaminaka *et al.*, "Diagnosis of C8 radiculopathy by magnetospinogram," *J. Neurol. Sci.*, vol. 405, no. 4, p. 34, 2019.
[168] T. Watanabe *et al.*, "Novel functional imaging technique for the brachial plexus based on magnetoneurography," *Clin. Neurophysiol.*, vol. 130, no. 11, pp. 2114–2123, 2019.
[169] B.-M. Mackert *et al.*, "Magnetoneurography of evoked compound action currents in human cervical nerve roots," *Clin. Neurophysiol.*, vol. 112, no. 2, pp. 330–335, 2001.
[170] M. Akaza *et al.*, "Noninvasive measurement of sensory action currents in the cervical cord by magnetospinography," *Clin. Neurophysiol.*, vol. 132, no. 2, pp. 382–391, 2021.
[171] B.-M. Mackert *et al.*, "Magnetometry of injury currents from human nerve and muscle specimens using superconducting quantum interferences devices," *Neurosci. Lett.*, vol. 262, no. 3, pp. 163–166, 1999.
[172] R. B. Govindan, E. Siegel, S. Mckelvey, P. Murphy, C. L. Lowery, and H. Eswaran, "Tracking the changes in synchrony of the electrophysiological activity as the uterus approaches labor using magnetomyographic technique," *Reprod. Sci.*, vol. 22, no. 5, pp. 595–601, 2014.
[173] A. Furdea, H. Eswaran, J. D. Wilson, H. Preissl, C. L. Lowery, and R. B. Govindan, "Magnetomyographic recording and identification of uterine contractions using Hilbert-wavelet transforms," *Physiol. Meas.*, vol. 30, no. 10, pp. 1051–1060, 2009.
[174] J. Marquetand *et al.*, "Magnetomyography—New opportunities with optically pumped magnetometers," *Int. J. Bioelectromagn.*, vol. 23, no. 2, pp. 1–4, 2021.
[175] D. Devedeux, C. Marque, S. Mansour, G. Germain, and J. Duchêne, "Uterine electromyography: A critical review," *Amer. J. Obstetrics Gynecol.*, vol. 169, no. 6, pp. 1636–1653, 1993.
[176] C. Buhimschi, M. Boyle, and R. Garfield, "Electrical activity of the human uterus during pregnancy as recorded from the abdominal surface," *Obstetrics Gynecol.*, vol. 90, no. 1, pp. 102–111, 1997.

KEREN ZHU (Student Member, IEEE) received the B.S. degree in electronical and computer engineering from The Ohio State University, Columbus, OH, USA, in 2017, where she is currently pursuing the Ph.D. degree in electrical and computer engineering.

She is currently a Graduate Research Assistant with ElectroScience Laboratory, Columbus. From May 2021 to July 2021, she was a Student Intern with Altair Engineering Inc., Troy, MI, USA. Her main research interests include electromagnetics, antennas, and bio-medical sensors.

Ms. Zhu received the Pre-Graduate Scholarship at the IEEE Microwave Theory and Techniques Society in 2018. She received Distinguished Graduate Student Award from The Ohio State University Women in Engineering in 2018. She also received the Best Student Paper Award at the ElectroScience Laboratory Annual Awards Ceremony in 2021, and got the Third Placed in 3-min Thesis Contest Award during 11th Annual CERF Technical Meeting in 2020.

ASIMINA KIOURTI (Senior Member, IEEE) received the Diploma degree in electrical and computer engineering from the University of Patras, Patras, Greece, in 2008, the M.Sc. degree in technologies for broadband communications from University College London, London, U.K., in 2009, and the Ph.D. degree in electrical and computer engineering from the National Technical University of Athens, Athens, Greece, in 2013.

She is currently an Assistant Professor of Electrical and Computer Engineering with The Ohio State University and the ElectroScience Laboratory, Columbus, OH, USA. From 2013 to 2016, she served as a Postdoctoral Researcher and then a Senior Research Associate with ElectroScience Laboratory. During her career, she has coauthored one book, 12 book chapters, five granted patents, over 70 journal papers, and over 130 conference papers/abstracts. Her research interests include bio-electromagnetics, wearable and implantable antennas, sensors for body area applications, and functionalized e-textiles.

Dr. Kiourti has received several awards for her research activity, including The Ohio State University Early Career Distinguished Scholar Award in 2022, the NSF CAREER Award in 2021, the 40 Under 40 recognition by Columbus Business First in 2021, the URSI Young Scientist Award in 2018, the IEEE Engineering in Medicine and Biology Society Young Investigator Award in 2014, the IEEE Microwave Theory and Techniques Society Graduate Fellowship for Medical Applications in 2012, and the IEEE Antennas & Propagation Society Doctoral Research Award in 2011. She is currently serving as the Senior Editor of the IEEE OPEN JOURNAL OF ANTENNAS AND PROPAGATION, an Editor of the Bioelectromagnetics column of the *IEEE Antennas and Propagation Magazine*, and an Associate Editor for the IEEE TRANSACTIONS ON ANTENNAS AND PROPAGATION, the IEEE JOURNAL OF ELECTROMAGNETICS, RF AND MICROWAVES IN MEDICINE AND BIOLOGY, and the *IEEE Antennas and Propagation Magazine*.